IEEE Access
Multidisciplinary ⋮ Rapid Review ⋮ Open Access Journal

Received 6 February 2024, accepted 13 March 2024, date of publication 18 March 2024, date of current version 27 March 2024.

Digital Object Identifier 10.1109/ACCESS.2024.3378733

RESEARCH ARTICLE

System Design of Cavity Resonance-Enabled Wireless Power Transfer Based on Filter Design Theory

YOSHINOBU TAMURA[1], HIROMASA SAEKI[2], AND MASAYA TAMURA[1]
[1]Department of Electrical and Electronic Information Engineering, Toyohashi University of Technology, Toyohashi 441-8580, Japan
[2]Murata Manufacturing Company Ltd., Yasu 520-2393, Japan

Corresponding author: Masaya Tamura (tamura.masaya@ieee.org)

This work was supported in part by MIC/SCOPE under Grant 175106001, and in part by the Knowledge Hub Aichi Priority Research Project from Aichi Prefectural Government.

ABSTRACT This study aims to realize an efficient system operation using wireless sensor networks (WSNs), which have been increasing in demand in recent years. To achieve this, a cavity resonance-enabled wireless power transfer (CR-WPT) technique has been proposed. The CR-WPT system is a WPT system that utilizes the cavity resonance phenomenon inside the cavity. This study solves the impedance mismatch problem caused by the resonance frequency changes depending on the installation condition of objects in the cavity resonator, which results in a power transmission efficiency(PTE) decrease. We propose the implementation of J-inverters and additional resonators outside and inside the cavity resonator and the configuration of a three-stage band-pass filter(BPF) to achieve broadband matching. The EM analysis results show that adding the J-inverters and additional resonators produces three poles in the reflection characteristics, verifying the proposed system operates as a three-stage BPF. A broadwidth of the power-supply frequency is realized. With a 2 W power input in the 117–122 MHz band, the bandwidth was broadened from approximately 0.6 to 2.0 MHz, which is approximately thrice the bandwidth of the previous system.

INDEX TERMS Cavity resonators, wireless power transmission, wireless sensor networks, band-pass filters.

I. INTRODUCTION

The usage of wireless sensor networks (WSNs) has recently been introduced into our daily lives [1], [2], [3], [4], [5], [6], [7], [8]. WSNs are used in a wide range of applications, from monitoring inside structure's temperatures to monitoring production equipment in factories. The sensors comprising WSNs are powered by batteries; hence, periodic battery replacement is required for system operation. However, the battery replacement timing for each sensor is not always the same, and frequent battery replacements negatively affect the system productivity. The WSNs demand is expected to increase with the rapid spread and use of the Internet of Things, requiring battery replacement for a large number of sensors in the future. Wireless power transfer (WPT) has been proposed as a solution to this problem. The electric field coupling method for short distances and the rectenna method for wide area coverage have been proposed as WPT methods suitable for supplying power to mobile devices and outdoor sensors. The electric field coupling method is resistant to the transmitter and receiver misalignment and requires only the use of electrodes on opposite metal plates. It can be used for indoor WPT as the transmission distance is only a few centimeters. The rectenna method is a WPT approach that uses radio waves and can supply power if the radio waves can propagate. The power transmission efficiency decreases significantly when the power receiver is placed out of the line of sight [11], [12], [13], [14], [15]. Therefore, the WPT method, which utilizes the resonance phenomenon of the structure in which the sensor is installed, is attracting attention [16], [17], [18], [19], [20]. One proposed method is placing a pillar with a capacitor inside a metallic structure and resonating the electric field inside this structure [16], [17]. The advantages of this method include a high power

The associate editor coordinating the review of this manuscript and approving it for publication was Diego Masotti.

supply efficiency and an easy adjustment of the power supply frequency. In addition, a single transmitter can drive multiple sensors; thus, power transmission efficiency(PTE) can be achieved even when the sensors are located far away or out of sight from the transmitter. This method requires the installation of a pillar within the structure, which limits the location of sensors and equipment. Herein, we propose a WPT that utilizes the principle of a cavity resonator and the resonant modes generated inside a metallic structure [21], [22], [23]. In this method, low-frequency electromagnetic waves are confined within a structure made of metal mesh walls. High-frequency signals for wireless communication can be exchanged inside and outside the cavity resonator, making it suitable for remote monitoring of conditions within the structure. Another advantage is that a pillar does not need to be installed within the structure. The system assumes that manufacturing equipment and wireless sensors are inserted inside the cavity resonator and not that the human body is inserted. Previous studies have not focused on environmental changes inside the cavity resonator, such as changes in the number of power receivers [16], [17], [18], [19], [20], [21], [22]. In CR-WPT, the wave impedance changes depending on the installation state of objects inside the structure. Moreover, the optimum frequency for the power supply changes. This system uses the cavity resonance phenomenon; therefore, the frequency that can be used for the power supply is a very narrow band. In a system with a fixed power supply frequency, the PTE will drop to almost 0 %, if the resonance frequency changes. To solve this problem, this study proposes a system design based on wideband bandpass filter design theory to widen the transmission frequency without reducing PTE. It has not been proposed or proven that BPF theory can be applied to feed power to a receiver with resonators placed inside a large resonator space. The proposed method is a structure with a new resonance structure in the resonator, and it is not clear whether such a structure can be designed using BPF theory and J-inverter. As far as we could find, we could not find any such prior literature, and our study here is novel. Our study is novel here. With our novel design theory, a broadband of the feeding frequency can be achieved. The novelty of this study is the design theory that applied filter design theory to CR WPT. Other CR WPT systems have been designed by optimization, but proposal theory can design CR WPT systems theoretically.

This work demonstrates the theory using a gable-shaped cavity resonator with a 1500 mm width, 1800 mm depth, and 1960 mm height(Fig.1). This is a scaled-down model simulating a manufacturing section with safety fencing in a factory and is worked as a cavity resonator. The walls are made of a 10 mm square aluminum mesh.

II. SYSTEM CONFIGURATION AND DESIGN METHODOLOGY

This chapter describes the design method of the proposed system. First, the operating frequency of the WPT system is determined utilizing the cavity resonance. The resonance

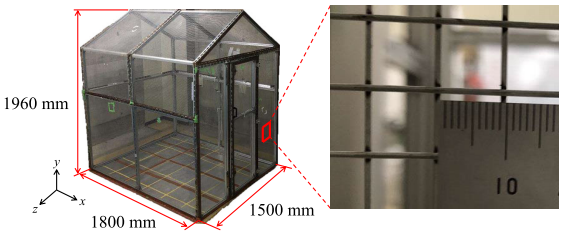

FIGURE 1. Cavity resonator with a mesh wall.

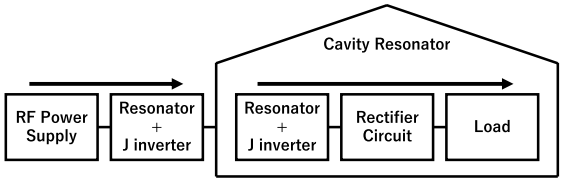

FIGURE 2. Basic configuration of the proposed system.

modes occurring in the cavity resonator are calculated, and the frequency at which the resonance mode produces a strong electric field in the range where the power supply is desired is adopted. Fig.2 depicts the basic configuration of the proposed system. Three resonators, namely, one cavity resonator and two resonators for incorporation are coupled by J-inverters. The J-inverter is a circuit element that converts the impedance. The proposed theory was verified using a cavity resonator with dimensions shown in Fig.1. In the CR-WPT system, the appropriate power transmitter and resonant circuit were mounted on the cavity resonator wall, while power receivers and resonators were positioned inside the cavity resonator. Fig.3 illustrates the equivalent circuit of the CR-WPT system. The equivalent circuit element values can be derived using circuit simulation software by fitting the gradient method so that the scattering matrices of the experiment and the equivalent circuit match. Fig.4 presents the equivalent circuit of the system in which the resonator is implemented in this equivalent circuit.

In order to design the proposed circuit, it is necessary to clarify the equivalent circuit parameters of only the cavity resonator. This chapter uses EM analysis to derive equivalent circuit element values. The position where the transmitter is inserted is shown in Fig.5. First, we calculate them using EM analysis. The transmitter and the receiver(Fig.6) were installed in the cavity resonator. Next, the element values with scattering matrices that matched the equivalent circuit in Fig.3 were derived. The transmitter and the receiver were mounted on FR-4 boards with 35 μm copper foils. The transmitter used a 100 mm$\times$100 mm substrate, while the receiver employed a 30 mm$\times$30 mm substrate. The size of the transmitter and receiver was set to the smallest size which would not lower the PTE while checking the result of the EM analysis. The scattering matrices obtained from the EM analysis software were fitted to the equivalent circuit in Fig.3. The frequency used for the WPT was in the 120 MHz band, which is the TE_{110} mode that occurs in the cavity in Fig.1. This is the dominant resonant mode in which dense regions of electric field occur throughout

the cavity [23]. The equivalent circuit element values were derived using the gradient method in the circuit analysis software. Table 1 lists the derived element values. The C_{TX} and C_{RX} were open stub-like elements that depended on the size and length of the transmitter and receiver, respectively. C_{12} denotes the electric field(J-inverter) coupling between the transmitter and the cavity resonator. C_{23} denotes the electric field(J-inverter) coupling between the receiver and the cavity resonator. C_{12} and C_{23} vary with the electrode dimensions of the transmitter and receiver respectively. C_{r2}, L_{r2}, and R_{r2} represent the cavity resonance phenomena of the TE_{110} mode. These values varied depending on the mode used. From the obtained element values, additional resonators and J-inverters shown in Fig.4 are designed using equation (1)–(6). Conventional CR-WPT systems use matching circuits to suppress the power reflections at only one frequency. The proposed system can set arbitrary bandwidth and PTE as numerical values by applying the theoretical design equation of the resonant coupled band-pass filter(equation (1)–(6)) to the CR-WPT system.

$$\omega_0 C_{ri} = \begin{cases} \dfrac{\omega_0^2 g_1 g_2 C_{12}^2}{w^2 \omega_0 C_{r2}} & (i = 1) \quad (1) \\ \dfrac{\omega_0^2 g_2 g_3 C_{23}^2}{w^2 \omega_0 C_{r2}} & (i = 3) \quad (2) \end{cases}$$

$$J_{i,i+1} = \begin{cases} \sqrt{\dfrac{\omega_0 w C_{r1}}{g_0 g_1 Z_A}} & (i = 0) \quad (3) \\ \sqrt{\dfrac{\omega_0 w C_{r3}}{g_3 g_4 Z_B}} & (i = 3) \quad (4) \end{cases}$$

$$C_{i,i+1} = \begin{cases} \dfrac{J_{01}}{\omega_0 \sqrt{1 - (J_{01} Z_A)^2}} & (i = 0) \quad (5) \\ \dfrac{2J_{34}}{\omega_0 \sqrt{1 - (J_{34} Z_B)^2}} & (i = 3) \quad (6) \end{cases}$$

where ω_0 is an angular center frequency; g_i is the i-th g-parameter; w is the specific bandwidth; and impedances Z_A and Z_B denote the input and output ports, respectively. The ω_0 was set to 119.3 [rad/s] from the WPT frequency. The g-parameters were calculated with Chebyshev characteristics of 0.46 dB ripple, 2.0 MHz bandwidth, 50 Ω input port impedance, and 100 Ω output port impedance. Then, from (1) to (6), the element values of the newly added resonator and J-inverter were designed using the g-parameters and WPT frequency. To operate the WPT system as a BPF, the design frequency was set to the WPT frequency. The input/output impedance was determined so that the fabricated prototype could be measured with a vector network analyzer(VNA). The bandwidth is wider than conventional, and the ripple is set to the smallest possible value. The element values of the equivalent circuits shown in Tables 1 and Table 2 were calculated by respectively fitting the EM analysis results and the measured results to the equivalent circuits. Then, from equation (1) to (6), the element values of the newly added resonator and J-inverter were designed using the g-parameters. The designed elements were attached to the transmitter and receiver, and EM analysis was performed. The resonant circuit connected to the analytical model of the transmitter and receiver is shown in Fig.6. Fig.7 presents the results(S_{11}) of setting the element values obtained by the equivalent circuitization and resonator design to the EM analysis model. In Fig.7(a), the proposed method generated three poles, which the conventional method matched at a single frequency point. In Fig.7(b) proposed method operated with the three resonators coupled with electromagnetic fields, whereas the conventional method operated in such a way that they could be matched at a single point. A discussion of experimental and analytical errors will be added as an error analysis. The average error between the circuit analysis and EM analysis was 7.42pt. The error is caused by the resonance frequency of added resonance circuits changed due to the effect of transmission lines. The abovementioned results show that the CR-WPT system can be designed based on the filter design theory from the EM analysis.

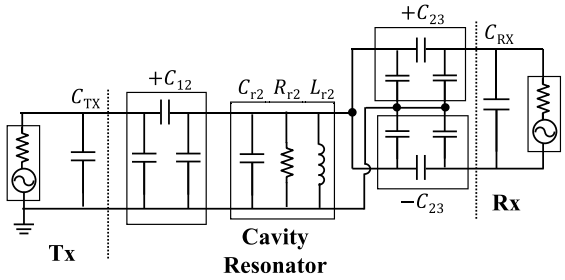

FIGURE 3. Equivalent circuit of the system.

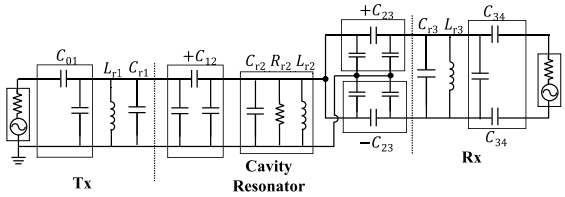

FIGURE 4. Equivalent circuit with additional circuits.

TABLE 1. The values of equivalent circuit elements for CR-WPT(Analysis).

Parameter	Value
C_{TX}	10.4 pF
C_{RX}	1.31 pF
C_{12}	0.571 pF
C_{23}	0.163 pF
C_{r2}	23.1 pF
L_{r2}	77.0 nH
R_{r2}	50.4 kΩ

III. EQUIVALENT CIRCUIT METHOD IN THE EXPERIMENTS

As revealed in the previous section, the equivalent circuitization is necessary for the CR-WPT system design based

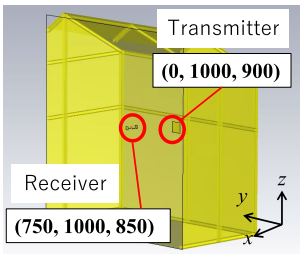

FIGURE 5. Placement of transmitter and receiver in EM analysis.

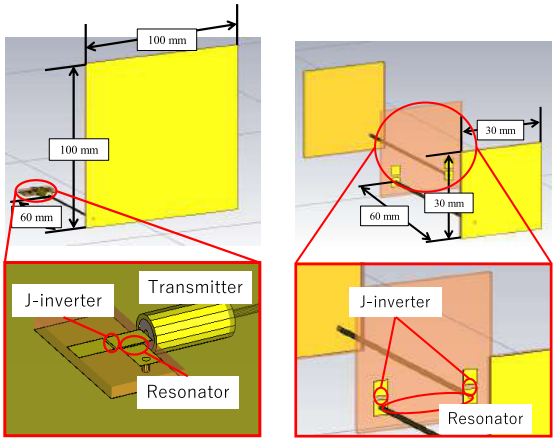

(a) power transmitter (b) power receiver

FIGURE 6. Transmitter and receiver geometries.

on the filter design theory. However, it was not possible to measure the scattering matrix on the receiver side inside the cavity. Only the scattering matrix on the transmitter side can be measured. In the proposed method, the value of the load connected to the power-receiving device is varied in multiple patterns, and the equivalent circuit element values are estimated from the one-port measurement results of multiple patterns. The F-matrix in Fig.3 is calculated as follows using equation (7).

$$F = \begin{pmatrix} a & b \\ c & d \end{pmatrix} \tag{7}$$

$$S_{11} = \frac{a\sqrt{\frac{Z_B}{Z_A}} + \frac{b}{\sqrt{Z_A Z_B}} - c\sqrt{Z_A Z_B} - d\sqrt{\frac{Z_A}{Z_B}}}{a\sqrt{\frac{Z_B}{Z_A}} + \frac{b}{\sqrt{Z_A Z_B}} + c\sqrt{Z_A Z_B} + d\sqrt{\frac{Z_A}{Z_B}}} \tag{8}$$

With the F to S matrix conversion, the scattering matrix on the transmitter side is expressed in equation (8). From equation (8), in which the scattering matrix on the transmitter side varies with the port impedance on the receiver side. Therefore, to derive the element values of the equivalent circuit from the measurement results, Z_B was varied to the seven patterns of 24, 51, 100, 150, 201, 300, and 1000 Ω, and one-port measurement was performed. Fig.8 shows the setup in which the scattering matrix is measured in one-port. The equivalent circuit of the differential power receiver was indirectly calculated by deriving the element values matching the equivalent circuit of the obtained one-port measurement results in Fig.3. Table 2 presents the equivalent circuitization results. The proposed theory of equivalent circuitization is considered to be correct, as it is in close agreement with the results of the EM analysis, Table 1. The above results indicate that the proposed equivalent circuit method for the actual device was completed and the equivalent circuit element values were estimated.

TABLE 2. The values of equivalent circuit elements for CR-WPT(Experiment).

Par	Value
C_{TX}	10.2 pF
C_{RX}	1.76 pF
C_{12}	0.762 pF
C_{23}	0.159 pF
C_{r2}	28.0 pF
L_{r2}	63.9 nH
R_{r2}	41.3 kΩ

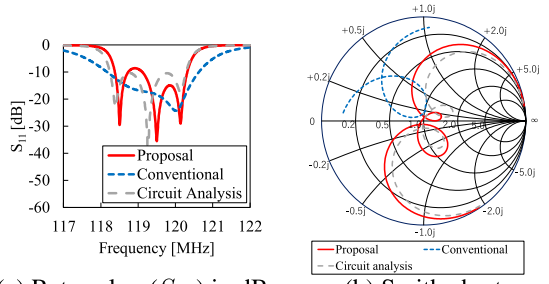

(a) Return loss(S_{11}) in dB (b) Smith chart

FIGURE 7. Analysis results of adding resonators to EM analysis software.

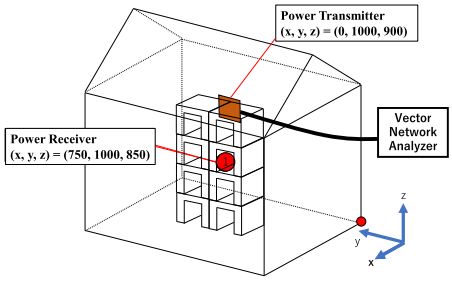

FIGURE 8. One-port measurement setup.

IV. MEASUREMENT OF THE SCATTERING MATRIX ON REAL EQUIPMENT

In this chapter, the external resonators were designed and experimented with based on the filter design theory. Fig.9 illustrates the transmitter and the receiver with the fabricated resonators and J-inverters. The meander-shaped transmitter and spiral-shaped receivers were used in previous studies [23]. However, the patch shape shown in Fig.9 did not significantly change the scattering matrix, so the patch shape was adopted for ease of fabrication. Again, the size of the transmitter and receiver was set to the smallest size which would not lower the PTE while checking the results of

the EM analysis. The resonators for implementation in the power transmitter and the receiver were designed using the equivalent circuit element values presented in Table 2 and equations (1) to (6). A resonator with three stages, 0.46 dB ripple, 2 MHz bandwidth, and 118.9 MHz center frequency obtained from the one-port measurement was designed and optimized to have a high PTE using the equivalent circuit analysis. Table 3 shows the resulting element values. The structure of the additional resonator is shown in Fig. 10. The additional resonator was constructed using chip element capacitors and air-core inductors, taking into account the effect of the Q–value. Fig.11 shows the measurement results of the scattering matrix when the LC components shown in Table 3 are mounted on a board. Theoretically, there should be three poles, but in Fig.11(a) there are two. The Smith chart for Fig.11(b) depicts that it behaved as if one pole was reduced from the trajectory in Fig.7. It is considered that the two poles are due to the low Q factor of the inductor and variations in the element values of C_{12} and C_{23}. The inductors were hand-wound and yielded a Q-factor of approximately 150 at around 120 MHz. The capacitors were chip elements with a Q-factor of approximately 3000. The low Q-factor of the inductor was the reason for the two poles.

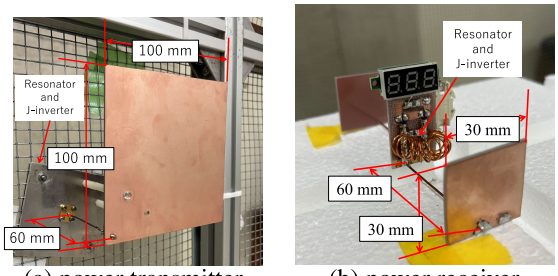

(a) power transmitter (b) power receiver

FIGURE 9. Transmitter and receiver with resonators and *J*-inverter.

TABLE 3. Resonator newly implemented and *J*-Inverter element values.

Parameter	Value
C_{01}	7.31 pF
C_{34}	2.17 pF
L_{r1}	20.2 nH
C_{r1}	54.2 pF
L_{r3}	514 nH
C_{r3}	0.100 pF

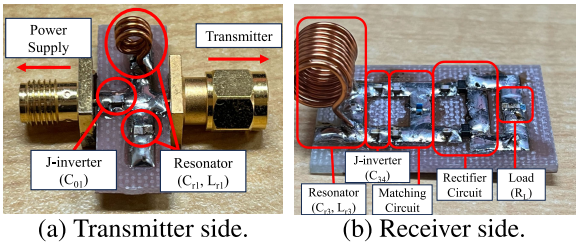

(a) Transmitter side. (b) Receiver side.

FIGURE 10. Additional resonator structures.

Fitting the equivalent circuit in Fig.4 to the experimental results, a circuit analysis of the PTE yielded the results demonstrated in Fig.12, suggesting that a PTE of approximately 50% can be obtained. The PTE is derived from S_{21} obtained by circuit analysis as in equation(9).

$$\mathrm{PTE} = S_{21} \times S_{21} \times 100[\%] \tag{9}$$

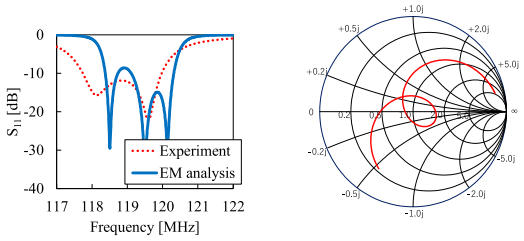

(a) Return loss(S_{11}) in dB (b) Smith chart

FIGURE 11. Experimental results with additional resonators.

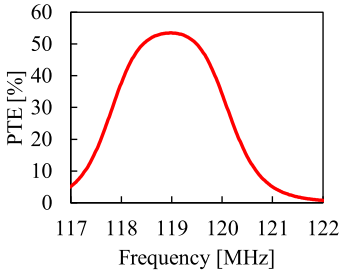

FIGURE 12. Circuit analysis of WPT.

V. CONFIRMATION OF POLES IN THE EXPERIMENT

This chapter, confirms the generation of three poles in the actual machine, which was not confirmed in the previous section. The two poles in the previous section were generated due to the low Q-factor of the device for implementation and the element value variation of C_{12} and C_{23}. Accordingly, the transmitter and the receiver were fabricated and adjusted, such that C_{12} and C_{23} had the same value. The designs of the resonators and J-inverters were not changed, only the electrode sizes of the transmitter and receiver were changed. The experiment was conducted using the transmitter and receiver shown in Fig.13. These were expected to result in C_{12} and C_{23} values close to those of the simulation. The equivalent system circuitization by the fitting as before resulted in the element values shown in Table 4. The resonance circuit designed by equation (1)–(6) was implemented. The scattering matrix was then measured and the results are shown in Fig.14. The figure shows three generated poles and three circles on the Smith chart. Therefore, it can be seen that in the actual device, a total of three resonators, consisting of a cavity and two additional resonators, are combined to operate as a bandpass filter.

VI. DESIGN AND MEASUREMENT OF RECTIFIER CIRCUITS

To provide DC power to a load, a rectifier circuit must be connected to the power receiver. Rectification is performed herein using the voltage doubler rectifier circuit shown in

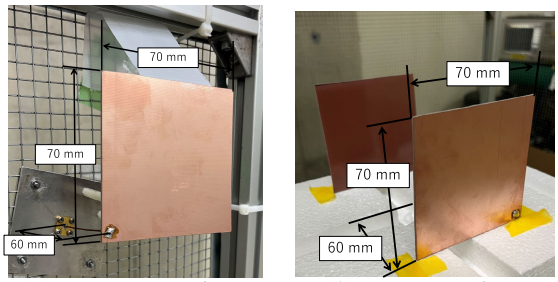

(a) Power transmitter (b) Power receiver

FIGURE 13. Transmitter and receiver shapes.

TABLE 4. The values of equivalent circuit elements for CR-WPT(Experiment).

Parameter	Value
C_{TX}	7.75 pF
C_{RX}	4.33 pF
C_{12}	0.495 pF
C_{23}	0.593 pF
C_{r2}	26.4 pF
L_{r2}	68.1 nH
R_{r2}	39.5 kΩ

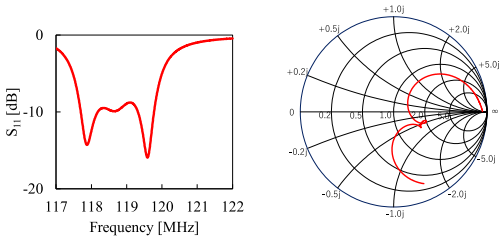

(a) Return loss(S_{11}) in dB (b) Smith chart

FIGURE 14. Results of connecting the resonator to the actual machine.

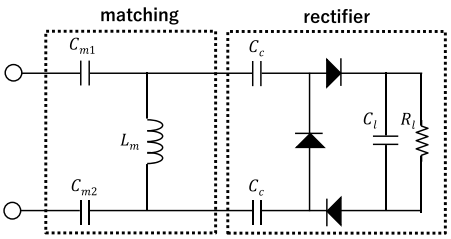

FIGURE 15. Circuit diagram of a voltage doubler rectifier circuit.

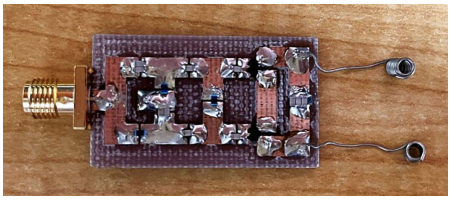

FIGURE 16. Voltage doubler rectifier circuit.

Fig.15. In the circuit, a matching circuit is inserted in its first stage because the input impedance of the rectifier circuit alone is far from 100 Ω, and connecting it directly to the electrode resulted in a large power reflection. A rectifier circuit with 100 Ω input and 2500 Ω output was realized by implementing the element values listed in Table 5.

Fig.16 shows the rectifier circuit. The output resistance of 2500Ω was adopted, which has the highest rectification efficiency based on circuit analysis of load characteristics. A balun circuit for the rectification efficiency measurement was connected to the circuit in Fig.16. The frequency was designed to provide the highest commutation efficiency at 120 MHz. Fig.17 shows an experimental system for measuring the rectification efficiency of a rectifier circuit. The circuit analysis and experiment results obtained from implementing the elements in Table 5 to Fig.18 are provided here. Both the experimental and analytical results were in excellent agreement with each other, depicting rectification efficiencies of 40%–60%. The power consumed by the load is proportional to the square of the voltage, so the higher the voltage, the greater the error. In other words, the RF–DC efficiency is the result of multiplying the RF–RF efficiency in Fig.12 by the rectification efficiency, defined as the WPT efficiency of the proposed system. The operation of the rectifier circuit obtained from the circuit analysis is shown in Fig.19. The output voltage V_{out} is approximately twice the differential voltage V_{in} input to the rectifier circuit.

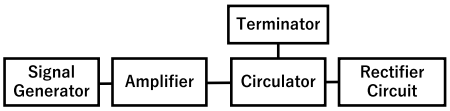

FIGURE 17. Experimental system for rectifier circuits.

TABLE 5. Rectifier circuit element values.

Parameter	Value
C_{m1}	15.5 pF
C_{m2}	11.8 pF
L_m	227.4 nH
C_{c}	22.0 pF
C_{l}	100 pF
R_{L}	2500 Ω

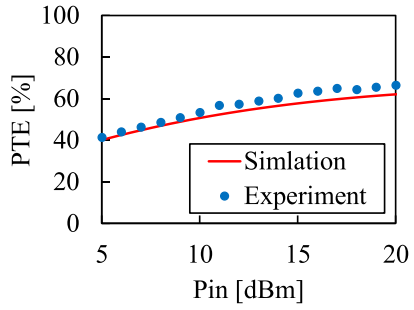

FIGURE 18. Rectification efficiency.

VII. POWER TRANSMISSION EXPERIMENT

In this chapter, WPT was performed from the transmitter to the receiver. Fig.20 and 21 illustrate the CR-WPT system used in the experiment. In this study, 2 W power at 120 MHz was applied to the cavity. The signal generator frequency was swept between 116 and 122 MHz in 0.2 MHz steps.

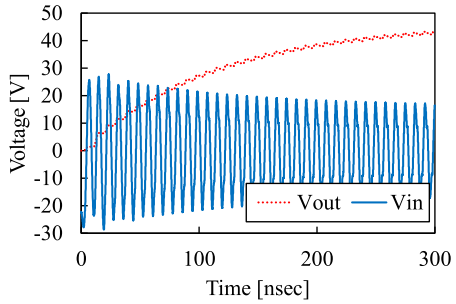

FIGURE 19. Rectifier circuit operation.

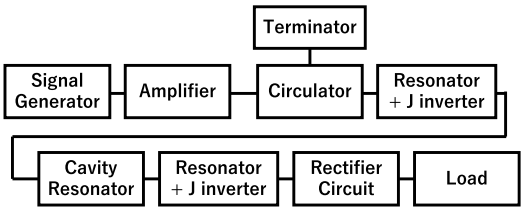

FIGURE 20. CR-WPT block diagram.

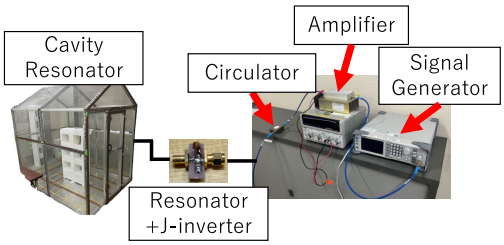

FIGURE 21. Experiment environment.

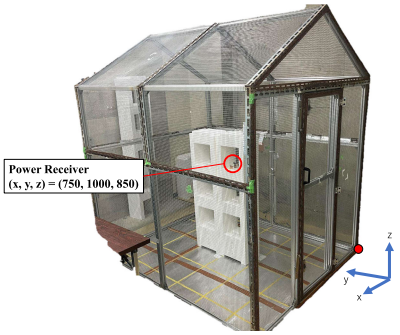

FIGURE 22. Position of a single power receiver.

First, the PTE was measured for the single power receiver. Then, a power transmission experiment was conducted with the receiver installed at the position shown in Fig.22. Fig.24 presents the RF–RF efficiency obtained by the circuit analysis software and experiments. The average error between the circuit analysis and the experimental results for the RF–RF efficiency is 1.5 pt, indicating that the PTE works as expected. The electric field distribution calculated by the EM simulator is shown in Fig.23. The closer to the center in the cavity resonator, the stronger the electric field is obtained. RF–RF efficiency (PTE) is derived as in equation (10) using V_{out} measured by the voltmeter of the receiver, the load resistance R_L, and the rectification efficiency η_{RC} of the rectifier circuit. The circuit analysis and experimental results showed a close agreement, proving that the equivalent circuit configuration was correct and operated according to theory.

Next, a comparison with the conventional method was performed [23]. The case involving the installation of one power receiver in a cavity was compared with that involving the installation of eight power receivers. Fig.25 demonstrates the installation position with an increased number of receivers. Fig.26 shows the RF–DC efficiencies obtained. In Fig.26(a), the proposed method had a wider bandwidth and a higher maximum efficiency than the conventional method. High efficiency can be achieved with the proposed method bandwidth, even if the frequency at which the maximum efficiency can be achieved shifts due to the changes in the environment inside the cavity resonator(e.g., an increase in the number of power receivers in Fig.26(b)). The proposed method achieved an efficiency of approximately 10% at 119.5–121 MHz, indicating that it can achieve almost the same characteristics as the system with a fixed feed frequency of 119 MHz. A comparison of bandwidths shows that efficiencies of more than 10% can be achieved at a wider range of frequency than with conventional ones.

TABLE 6. PTE at the feeding frequency of 118.8 MHz.

Index	Conventional	Proposal
Rx1	31.3 %	30.3 %
Rx2	31.2 %	31.4 %
Rx3	25.3 %	30.2 %
Rx4	7.02 %	17.1 %

TABLE 7. Comparision of reported WPT system.

	Frequency	Rx Size	PTE (RF–RF)	Fractional bandwidth
[16]	1.32 MHz	165 mm	70 %	N/A
[18]	191.65 MHz	76 mm	60 %	1.38 %
[19]	335.0 MHz	7 mm	14.32 %	0.231 %
[20]	278 MHz	40 mm	85.3 %	N/A
This work	120 MHz	30 mm	53.1 %	1.85 %

TABLE 8. Comparision of other methods of WPT system.

	Method	Efficiency	Input Power	Change in number of Rx
[12]	Rectenna	28.0 % (RF–DC)	-15 dBm	N/A
[14]	Rectenna	35.0 % (RF–DC)	16 dBm	N/A
[18]	CR-WPT	30 % (RF–DC)	39 dBm	N/A
[19]	CR-WPT	14.32 % (RF–RF)	33 dBm	N/A
This work	CR-WPT	35.1 % (RF–DC)	33 dBm	Yes

This is followed by verification against the strength of the position misalignment of the receiver. The receivers are placed in turn at the four locations in the cavity resonator shown in Fig.27 and the change in PTE is measured. Fig.28 shows the results of the strength of the position shift for the conventional and proposed methods. The PTE at a feed frequency of 118.8 MHz is shown in Table 6. At three

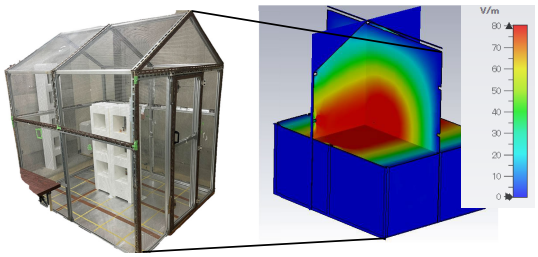

FIGURE 23. Electric field distribution in cavity resonators.

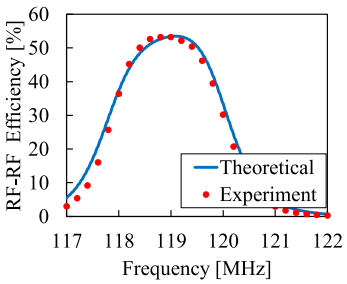

FIGURE 24. Efficiency comparison of the circuit analysis and experiments.

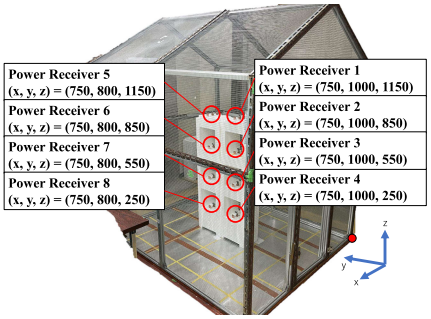

FIGURE 25. Positions of eight power receivers.

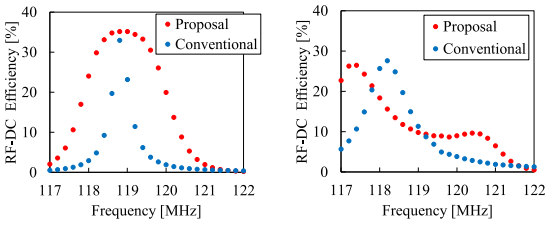

(a) One power receiver (b) Eight power receivers

FIGURE 26. Difference in the efficiency depending on the number of power receivers(RF-DC efficiency).

positions, the PTE was found to be improved by the proposed method over the conventional method and was found to be more resistant to the position misalignment of the receiver than the conventional method.

Compared with conventional methods, a wideband system can be built with a single receiver. As the number of receivers increases, the peak value of PTE shifts to lower frequencies than before. However, it has the advantage of being able to provide WPT with higher efficiency for larger spaces than previously possible. Comparisons with other studies are shown in Table 7. There is a trade-off between the size of the receiver and the PTE. A comparison of the fractional

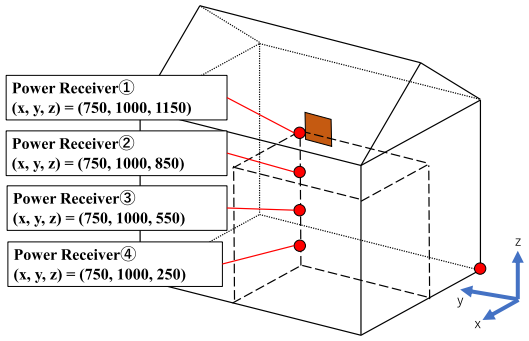

FIGURE 27. Position of the receiver to verify the strength of the position misalignment.

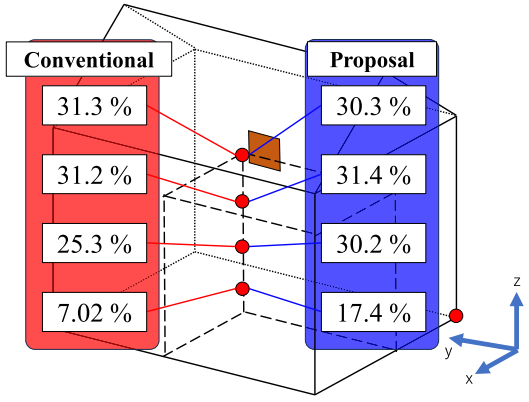

FIGURE 28. PTE at each position.

bandwidth shows an improvement over previous studies. Therefore, it is possible to supply power to numerous power receivers without adjusting external circuits. Table 8 shows a comparison with other WPT systems. The advantage of the rectenna method is that the feed frequency does not change depending on the number of power receivers, but the input power available is restricted by law and efficiency is low. This makes it difficult to charge several sensors at a time. CR WPT can input power higher than the rectenna method due to the suppression of leakage electromagnetic fields [23] because the power is transmitted within a shielded space. This means that power can be supplied to many sensors at once. The proposed method maintains high efficiency even with variations in the number of power receivers, as opposed to other CR WPT systems that are specifically tuned to a certain frequency. It is believed that the proposed method is more suitable for WSNs than other methods.

$$\mathrm{PTE} = \frac{V_{out}^2}{P_{in} \times R_L \times \eta_{RC}} \times 100[\%] \tag{10}$$

VIII. CONCLUSION

This study developed a design theory of systems based on the design theory of filters to popularize systems that use WSNs. First, the CR-WPT system was modeled and made into an equivalent circuit using the EM analysis software. Next, the obtained equivalent circuit element values were combined with the band-pass filter design theory to design

a resonant circuit for incorporation into the CR-WPT system. Three poles were generated after the appropriate elements were set, and an EM analysis was performed. The filter design theory can clearly be theoretically applied. The transmission experiments showed that the proposed method can achieve a bandwidth of 2.0 MHz while the conventional method can achieve a PTE of 20% at approximately 0.6 MHz, which is approximately thrice its bandwidth.

REFERENCES

[1] G. Lee and G. Ahn, "Wireless power transfer of daisy chain structure on rotating spindle," in *Proc. IEEE Wireless Power Transf. Conf. (WPTC)*, Nov. 2020, pp. 384–3876.

[2] S. W. Dong, "Hybrid mode wireless power transfer for wireless sensor network," in *Proc. IEEE Wireless Power Transf. Conf. (WPTC)*, 2019, pp. 561–564.

[3] A. O. Almagrabi, "Fair energy division scheme to permanentize the network operation for wireless rechargeable sensor networks," *IEEE Access*, vol. 8, pp. 178063–178072, 2020, doi: 10.1109/ACCESS.2020.3027615.

[4] N. Khalid, R. Mirzavand, H. Saghlatoon, M. M. Honari, and P. Mousavi, "A three-port zero-power RFID sensor architecture for IoT applications," *IEEE Access*, vol. 8, pp. 66888–66897, 2020, doi: 10.1109/ACCESS.2020.2985711.

[5] J. Chen, C. W. Yu, and W. Ouyang, "Efficient wireless charging pad deployment in wireless rechargeable sensor networks," *IEEE Access*, vol. 8, pp. 39056–39077, 2020, doi: 10.1109/ACCESS.2020.2975635.

[6] T.-H. Tsai, C.-C. Huang, C.-H. Chang, and M. A. Hussain, "Design of wireless vision sensor network for smart home," *IEEE Access*, vol. 8, pp. 60455–60467, 2020, doi: 10.1109/ACCESS.2020.2982438.

[7] I. Yoon and D. K. Noh, "Adaptive data collection using UAV with wireless power transfer for wireless rechargeable sensor networks," *IEEE Access*, vol. 10, pp. 9729–9743, 2022, doi: 10.1109/ACCESS.2022.3144846.

[8] M. Poveda-García, J. Oliva-Sánchez, R. Sanchez-Iborra, D. Cañete-Rebenaque, and J. L. Gomez-Tornero, "Dynamic wireless power transfer for cost-effective wireless sensor networks using frequency-scanned beaming," *IEEE Access*, vol. 7, pp. 8081–8094, 2019, doi: 10.1109/ACCESS.2018.2886448.

[9] A. Muharam, S. Ahmad, R. Hattori, and A. Hapid, "13.56 MHz scalable shielded-capacitive power transfer for electric vehicle wireless charging," in *Proc. IEEE PELS Workshop Emerg. Technologies: Wireless Power Transf. (WoW)*, Seoul, South Korea, Nov. 2020, pp. 298–303, doi: 10.1109/WoW47795.2020.9291299.

[10] B. Regensburger, A. Kumar, S. Sinha, and K. Afridi, "High-performance 13.56-MHz large air-gap capacitive wireless power transfer system for electric vehicle charging," in *Proc. IEEE 19th Workshop Control Model. for Power Electron. (COMPEL)*, Padua, Italy, Jun. 2018, pp. 1–4, doi: 10.1109/COMPEL.2018.8460153.

[11] S. T. Khang, D. J. Lee, I. J. Hwang, T. D. Yeo, and J. W. Yu, "Microwave power transfer with optimal number of rectenna arrays for midrange applications," *IEEE Antennas Wireless Propag. Lett.*, vol. 17, no. 1, pp. 155–159, Jan. 2018.

[12] V. Palazzi, C. Kalialakis, F. Alimenti, P. Mezzanotte, L. Roselli, A. Collado, and A. Georgiadis, "Design of a ultra-compact low-power rectenna in paper substrate for energy harvesting in the Wi-Fi band," in *Proc. IEEE Wireless Power Transf. Conf. (WPTC)*, May 2016, pp. 1–4.

[13] N. Takabayashi, K. Kawai, M. Mase, N. Shinohara, and T. Mitani, "Large-scale sequentially-fed array antenna radiating flat-top beam for microwave power transmission to drones," *IEEE J. Microw.*, vol. 2, no. 2, pp. 297–306, Apr. 2022, doi: 10.1109/JMW.2022.3157845.

[14] B. T. Malik, V. Doychinov, A. M. Hayajneh, S. A. R. Zaidi, I. D. Robertson, and N. Somjit, "Wireless power transfer system for battery-less sensor nodes," *IEEE Access*, vol. 8, pp. 95878–95887, 2020, doi: 10.1109/ACCESS.2020.2995783.

[15] M. K. Hosain, A. Z. Kouzani, M. F. Samad, and S. J. Tye, "A miniature energy harvesting rectenna for operating a head-mountable deep brain stimulation device," *IEEE Access*, vol. 3, pp. 223–234, 2015, doi: 10.1109/ACCESS.2015.2414411.

[16] T. Sasatani, M. Chabalko, Y. Kawahara, and A. Sample, "Geometry-based circuit modeling of quasi-static cavity resonators for wireless power transfer," *IEEE Open J. Power Electron.*, vol. 3, pp. 382–390, 2022.

[17] Z. Yue, Q. Zhang, D. Zhao, and B.-Z. Wang, "A non-radiative wireless power transfer based on sparse quasi-static cavity resonator," in *Proc. Int. Appl. Comput. Electromagn. Soc. (ACES-China) Symp.*, Jul. 2021, pp. 1–2.

[18] M. J. Chabalko and A. P. Sample, "Three-dimensional charging via multimode resonant cavity enabled wireless power transfer," *IEEE Trans. Power Electron.*, vol. 30, no. 11, pp. 6163–6173, Nov. 2015.

[19] H. Mei, K. A. Thackston, R. A. Bercich, J. G. R. Jefferys, and P. P. Irazoqui, "Cavity resonator wireless power transfer system for freely moving animal experiments," *IEEE Trans. Biomed. Eng.*, vol. 64, no. 4, pp. 775–785, Apr. 2017.

[20] Z. Yue, Q. Zhang, Z. Yang, R. Bian, D. Zhao, and B.-Z. Wang, "Wall-meshed cavity resonator-based wireless power transfer without blocking wireless communications with outside world," *IEEE Trans. Ind. Electron.*, vol. 69, no. 7, pp. 7481–7490, Jul. 2022, doi: 10.1109/TIE.2021.3102453.

[21] M. Tamura, D. Furusu, and I. Takano, "Wireless power and information transfer in closed space utilizing frequency selected surfaces," in *IEEE MTT-S Int. Microw. Symp. Dig.*, Jun. 2017, pp. 1046–1049.

[22] S. Nimura, D. Furusu, and M. Tamura, "Improvement in power transmission efficiency for cavity resonance-enabled wireless power transfer by utilizing probes with variable reactance," *IEEE Trans. Microw. Theory Techn.*, vol. 68, no. 7, pp. 2734–2744, Jul. 2020.

[23] S. Akai, H. Saeki, and M. Tamura, "Power supply to multiple sensors and leakage field analysis using cavity resonance-enabled wireless power transfer," in *IEEE MTT-S Int. Microw. Symp. Dig.*, Denver, CO, USA, Jun. 2022, pp. 271–274, doi: 10.1109/IMS37962.2022.9865566.

YOSHINOBU TAMURA received the B.E. degree in electrical and electronic information engineering from Toyohashi University of Technology, Toyohashi, Japan, in 2022, where he is currently pursuing the master's degree. He is engaged in the development of wireless power transmission systems in enclosed space.

HIROMASA SAEKI received the B.E. and M.E. degrees in condensed matter physics from Osaka University, Osaka, Japan, in 2000 and 2002, respectively. From 2001 to 2003, he was a Research Fellow with Japan Society for the Promotion of Science. From 2004 to 2006, he was a Research Assistant with Osaka University. In December 2006, he joined Murata Manufacturing Company Ltd., where he was involved in the development of SAW filters, light emitting diodes, thin film capacitors, and wireless power transfers.

MASAYA TAMURA received the B.E. and M.E. degrees from Okayama University, Okayama, Japan, in 2001 and 2003, respectively, and the Ph.D. degree from Kyoto University, Kyoto, Japan, in 2012. From April 2003 to March 2014, he was with Panasonic Company Ltd., where he has been engaged in the research and development of high-frequency components, including light wave, especially microwave filters, metamaterials, and plasmonics. In April 2014, he joined Toyohashi University of Technology, where he is currently a Professor of electrical and electronic information engineering. His current research interests include microwave circuits and wireless power transfers. He was a recipient of the IEEE MTT-S Outstanding Young Engineer Award, in 2015. He also received the 2012 IEEE MTT-S Japan Young Engineer Award and the 2012 Michiyuki Uenohara Memorial Award.